Advances in Cement Research

ice publishing

Performance of plain and slag-blended cements and mortars exposed to combined chloride–sulfate solution

Joseph O. Ukpata
PhD Researcher, School of Civil Engineering, University of Leeds, Leeds, UK

P. A. Muhammed Basheer
Professor, School of Civil Engineering, University of Leeds, Leeds, UK

Leon Black
Associate Professor, School of Civil Engineering, University of Leeds, Leeds, UK (corresponding author: l.black@leeds.ac.uk)
(Orcid:0000-0001-8531-4989)

The durability of reinforced concrete structures exposed to aggressive environments remains a challenge to both researchers and the construction industry. This study investigates the hydration, mechanical properties and durability characteristics of ground granulated blast-furnace slag (GGBS) – blended cements and mortars exposed to a combined sodium chloride–sulfate environment, at temperatures of 20°C and 38°C. The conditions were chosen so as to assess the performance of slag blends under typical temperate and warm tropical marine climatic conditions. Slags with calcium oxide-to-silicon dioxide ratios of 1·05 and 0·94, were blended with CEM I 52.5R at 30% replacement level to study the influence of slag composition and temperature. Parallel control tests were carried out with CEM I 42.5R. Pastes and mortar samples were cast using 0·5 water-to-binder ratio, pre-cured for 7 d in water before exposure. Flexural strengths were determined when the samples were 7, 28 or 90 d old. Hydration was followed using X-ray diffraction (XRD), thermal analysis and calorimetry. Also, sorptivity, gas permeability and chloride diffusion tests were carried out on mortar samples to measure transport and durability characteristics. The results show improved mechanical and transport properties for slag blended cements exposed to environments rich in sodium chloride and sulfate.

Notation

A	cross-sectional area of specimen
CH_w	mass loss from portlandite (%)
C	chloride concentration
C_i	initial chloride concentration of the mortar
C_s	surface chloride concentration
$C(x, t)$	chloride ion concentration at a depth x from an exposed surface for time t
D	chloride diffusion coefficient
D_a	apparent chloride diffusion coefficient (mm²/year)
i	cumulative water absorption (g/mm²)
K_i	intrinsic gas permeability
k	sorptivity coefficient ((g/mm²)/s^{0·5})
L	length of specimen (m)
M_{Ag}	molarity of the silver nitrate solution
M_{CH}	molar mass of portlandite
M_{H_2O}	molar mass of water
m	mass of powder sample (g)
P_1, P_2	injection and exit pressures (Pa)
Q	volume flow rate of gas measured at pressure P_2 (m³/s)
t	time (s)
V_{Ag}	volume of silver nitrate added (cm³)
V_1, V_2	volumes of ammonium thyocyanate solution (cm³)
W_b	bound water (%)
W_{50}	residual mass at 50°C
W_{550}	residual mass at 550°C
μ	dynamic viscosity of gas at the test temperature (Ns/m²)

Introduction

Reinforced concrete is the most popular construction material globally. However, its performance in marine environments can be severely undermined by the actions of chlorides and sulfates present in seawater. Chlorides are typically known to cause the corrosion of embedded steel reinforcement bars by de-passivating the surrounding protective film created by the high alkalinity in cement hydration products (Galan and Glasser, 2015; Holden *et al.*, 1983), whereas sulfates tend to attack and weaken the binding property of cement in the concrete matrix due to the decalcification of the calcium silicate hydrate (C–S–H) gel (Bai *et al.*, 2003) and ettringite precipitation (Whittaker and Black, 2015).

The conjoint attack of cements by chloride and sulfate is still the subject of three conflicting views in the literature, with chlorides either accelerating, mitigating or having no impact on sulfate attack (Al-Amoudi *et al.*, 1995; Sotiriadis *et al.*, 2013). However, there appears to be a consensus concerning the influence of sulfate on chloride attack. Sulfates reduce the ingress of chloride into concrete at early ages due to ettringite formation, which gives rise to a compact microstructure. This trend is said to be reversed at later ages, however, possibly due to excessive formation of expansive ettringite crystals causing cracks that provide channels for rapid ingress of chlorides into concretes or mortars (Abdalkader *et al.*, 2015; Zuquan *et al.*, 2007). Frias *et al.* (2013) attributed improved early-age performance to the partial inhibition of Friedel's salt as sulfate reacts with calcium aluminate hydrates preferentially to

Advances in Cement Research
Volume 30 Issue 8

Performance of plain and slag-blended
cements and mortars exposed to
combined chloride–sulfate solution
Ukpata, Basheer and Black

precipitate non-expansive ettringite inside the pores. Sulfates are also known to reduce chloride binding by cement hydrates, leading to increased free chloride in the exposed mortar or concrete matrix (De Weerdt et al., 2014; Ehtesham Hussain and Rasheeduzzafar, 1994).

There are claims that blending Portland cement with slag results in greater chloride binding capacity due to increased Friedel's salt formation (Maes and De Belie, 2014; Otieno et al., 2014). Luo et al. (2003) suggested that the reduced influence of sulfate on chloride binding for slag blended cements may be due to the lower sulfate content in slags. Slags will also increase C–S–H formation, onto which chlorides can be adsorbed. Other researchers have also found that sulfate attack can be reduced by the incorporation of aluminium-rich slag in Portland cement systems (Whittaker et al., 2014, 2016), with minimal improvement in hydraulic reactivity and no negative effect on mechanical and durability properties (Herrero et al., 2016).

Besides reducing the carbon footprint of cement production, the incorporation of slag in Portland cement has gained much popularity due to its potential to enhance strength and durability. Slag reacts with water and calcium hydroxide from cement hydration to produce additional C–S–H gel, contributing to strength development. Also, slag is known to refine the pore structure of concrete through particle packing, causing densification, and thus, increased strength and durability. The reactivity of slag is dependent on its chemical composition (Ogirigbo and Black, 2016), with more basic slags known to be more reactive. Thus, both BS EN 15167-1 (BSI, 2006) and BS EN 197-1 (BSI, 2011) require a basicity ratio of $(CaO + MgO)/(SiO_2)$ to be greater than 1·0 for slags to be regarded as good for cement purposes. Other basicity ratios have also been suggested in the literature to determine the potential reactivity of slags, although their reliabilities in effectively predicting the reactivity of slags are still questioned (Mantel, 1994; Winnefeld et al., 2015).

Besides major oxides such as calcium oxide (CaO) and silicon dioxide (SiO_2), the roles of aluminium oxide (Al_2O_3) and magnesium oxide (MgO) in slag can significantly influence different performance requirements of slag blended cements. Increasing the magnesium oxide content in slag has been found to reduce porosity and increase strength for alkali-activated slags, while an increase in aluminium oxide was reported to show opposite results at early stage and insignificant effects at later age for hydration, compressive strength and coarse porosity, respectively (Haha et al., 2011, 2012; Winnefeld et al., 2015). However, aluminium content is important for chloride penetration resistance for slag blends (Otieno et al., 2014), and was found to have a considerable impact on strength development when the aluminium oxide content was increased from 8 to 12%, but had a lesser effect beyond 12 up to 16% (Kucharczyk et al., 2016).

Transport of aggressive species occurs primarily through the binder paste (Sabir et al., 1998), with some contribution from the interfacial transition zone (ITZ) (Basheer et al., 2005; Shen et al., 2017). Therefore, an understanding of the relationship between binder reactivity and transport properties will enable better application of slag cements in aggressive environments, for example seawater. Hence, this study focuses on the influence of slag chemical composition and temperature on hydration, mechanical properties and transport properties of slag blended cements exposed to attack by a combined sodium chloride and sulfate solution.

Experimental details

Materials
CEM I 52.5R was used to prepare slag blends at 30% replacement by weight. Two types of slags (compliant with BS EN 15167-1 (BSI, 2006)) (related to ASTM C 989 (ASTM, 2016)) were used, designated as slag 1 and slag 2 (Table 1). These slags had similar physical properties, but calcium oxide/silicon dioxide ratios of 1·05 and 0·94, respectively. The chemical compositions and physical properties of the test binders are shown in Tables 2 and 3, respectively. The particle size distributions of slags 1 and 2 are shown in Figure 1. A control mix was used comprising a CEM I 42.5R binder. This is in line with industrial practice, where higher strength grade of Portland cements are blended with supplementary cementitious materials (SCM) to derive lower grade binder. Natural sand sieved to maximum size of 2·0 mm was used to prepare mortar samples. Standard laboratory reagent grade sodium chloride (30 g/l) and sodium sulfate (3 g/l) were mixed to prepare the test solutions. The concentrations were chosen to reflect the concentrations of chloride and sulfate in typical seawater (Eglinton, 2004). All paste and mortar mixes and test solutions were prepared using deionised water.

Sample preparation and curing conditions
Mortar prisms (40 mm × 40 mm × 160 mm) were used to determine the flexural strength and the chloride profile and paste samples were used for the chemical and microstructural characterisation. The binder-to-aggregate ratio was 1:3, and water-to-binder (w/b) ratio was 0·5 (Table 4). Mortars were mixed for 4 min using an automatic mixer compliant with BS EN 196-1 (BSI, 2005) (related to ASTM C 305 (ASTM, 2014)). Mortar cylinders (28 mm dia. and 40 mm high) were used for sorptivity and gas permeability tests. The small size was adopted to accelerate the drying period to enable early-age measurements to be made. The samples were initially cast in plastic vials of 28 mm dia. by 50 mm, cured and cut to test size (40 mm thick) using a Struers Accutom-5, before conditioning in a ventilated oven set at 40°C (BS EN 13057 (BSI, 2002)) to constant mass. The laitance at the uncut end of each sample was removed by grinding on coarse silicon carbide papers grit 220 to expose the mortar pore structure. All mortar samples were demoulded after 24 h and cured in water for

Advances in Cement Research
Volume 30 Issue 8

Performance of plain and slag-blended
cements and mortars exposed to
combined chloride–sulfate solution
Ukpata, Basheer and Black

Table 1. Selected HIs

Hydraulic index (HI)	Slag 1	Slag 2	Requirement for good performance: %	Reference
CaO + MgO + SiO$_2$	83·37	87·55	≥66·7	BS EN 15167 (BSI, 2006)
(CaO + MgO)/SiO$_2$	1·28	1·18	<1·0	BS EN 15167 (BSI, 2006)
CaO/SiO$_2$	1·05	0·94	<1·0	Mantel (1994)

Table 2. Chemical properties of cementitious materials (as received from the manufacturers)

Property	Unit	CEM I 42.5R	CEM I 52.5R	Slag 1 (S1)	Slag 2 (S2)
Silicon dioxide (SiO$_2$)	%	20·17	20·50	36·58	40·14
Aluminium oxide (Al$_2$O$_3$)	%	5·33	5·43	12·23	7·77
Titanium dioxide (TiO$_2$)	%	0·29	0·29	0·83	0·30
Manganese oxide (MnO)	%	0·05	0·05	0·64	0·64
Iron (III) oxide (Fe$_2$O$_3$)	%	2·65	2·51	0·48	0·78
Calcium oxide (CaO)	%	63·01	63·43	38·24	37·90
Magnesium oxide (MgO)	%	1·45	1·51	8·55	9·51
Potassium oxide (K$_2$O)	%	0·76	0·79	0·65	0·55
Sodium oxide (Na$_2$O)	%	0·14	0·17	0·27	0·36
Sulfur trioxide (SO$_3$)	%	3·33	3·43	1·00	1·47
Phosphorus pentoxide (P$_2$O$_5$)	%	0·12	0·14	0·06	0·02
Loss on ignition (LOI) 950°C	%	2·12	1·37	+1·66	+0·40
Total	%	99·42	99·62	99·88	99·43
Glass content	%	na	na	99·3	97·1
CaO/SiO$_2$		na	na	1·05	0·94
(CaO + MgO)/SiO$_2$		na	na	1·28	1·18
Phase compositions					
C$_3$S	%	57·6	58·5	na	na
C$_2$S	%	15·0	14·4	na	na
C$_3$A	%	9·6	10·7	na	na
C$_4$AF	%	7·5	7·0	na	na
Calcite	%	2·7	0·8	na	na

Table 3. Physical properties of cementitious materials

Property	Unit	CEM I 42.5R	CEM I 52.5R	Slag 1 (S1)	Slag 2 (S2)
Blaine	cm^2/g	3490	7357	5995	5540
Density	g/cm^3	3·14	3·16	2·93	2·91
D10	μm	3·54	2·94	2·27	2·87
D50	μm	16·29	9·43	11·56	12·91
D90	μm	46·86	22·47	32·97	47·13

Figure 1. Particle size distribution of slags

further 6 d (except those for total chloride profile analysis). This curing regime was followed by immersion in combined chloride (30 g/l) and sulfate (3 g/l) solution maintained at either 20°C or 38°C up to test ages (i.e. 7, 28 and 90 d). This exposure condition is designated here as X2, corresponding to the XS2 standard exposure class for risk of corrosion caused by chlorides in seawater (BS EN 206 (BSI, 2013); BS 8500-1 (BSI, 2015a)). Parallel samples were also cured in water, designated as X1, to allow for comparison.

The prism samples for total chloride profile analysis were prepared according to BS EN 12390-11 (BSI, 2015b) (related to ASTM C 1543 (ASTM, 2010)) but with slight changes.
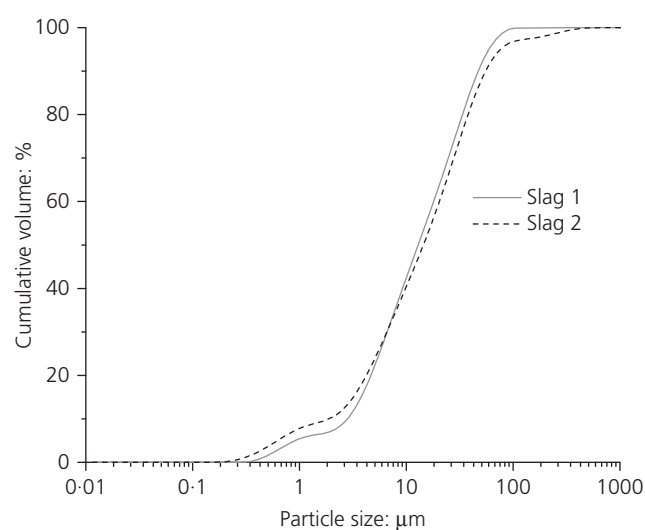
Mortar samples were pre-cured for 28 d under water, after which a 20 mm thick slice was cut off from one square end to expose the true pore structure of the mortar. The remaining

Advances in Cement Research
Volume 30 Issue 8

Performance of plain and slag-blended
cements and mortars exposed to
combined chloride–sulfate solution
Ukpata, Basheer and Black

Table 4. Mix ratios

| | | CEM I | | GGBS | | | |
Mix	w/b ratio	42.5R	52.5R	Slag 1	Slag 2	Water	Sand
C1	0·5	1	0	0	0	0·5	3
C2S1	0·5	0	0·7	0·3	0	0·5	3
C2S2	0·5	0	0·7	0	0·3	0·5	3

Figure 2. Cutting of mortar slices for chloride profile analysis

surfaces of each sample were coated with epoxy resin, to allow for unidirectional chloride diffusion. The samples were then left for 2 d to dry, followed by saturation in deionised water for about 24 h before immersion in the test solution, which was renewed monthly. The volume of the test solution was kept above 12·5 mm/cm^2 of exposed surface and the sample was stored for 90 d (BS EN 12390-11 (BSI, 2015b)). After the exposure period, seven parallel slices of approximately 5 mm thickness were obtained from each prism sample (see Figure 2), similar to Ogirigbo (2016), dried and ground to particle size passing a 150 μm sieve ready for chloride analysis. This method was found to be simpler and faster than conventional profile grinding methods (Bamforth *et al.*, 1997), and tends to provide a more representative result about the cross-section rather than a small portion covered in the profile grinding.

Paste samples were cast in 8 ml plastic vials using 0·5 w/b ratio for simultaneous thermal analysis (STA) and X-ray diffraction (XRD) analysis. The paste samples were exposed to a chloride-bearing (30 g/l) and sulfate-bearing (3 g/l) test solution as described earlier. Hydration was stopped at ages corresponding to strength tests using a three-step procedure comprising: iso-propanol solvent exchange of pore water, followed by washing with diethyl ether and 15 min drying on hot plate set at 40°C to evaporate any remaining diethyl ether (Lothenbach *et al.*, 2016). The dry samples were then kept under vacuum in a desiccator until analysis. Prior to each STA and XRD analysis,

the dry paste sample was ground to form an homogeneous fine powder of approximately 63 μm particle size, using an agate pestle and mortar.

Test methods

Setting time
Setting times of plain and blended pastes using 0·5 w/b ratio were obtained using an automatic setting time apparatus, in line with BS EN 196-3 (BSI, 2008) (related to ASTM C 191 (ASTM, 2013)). The Controls automatic Vicat apparatus was equipped with an in-water testing accessory, where the test specimen was submerged in circulating water below the needle, which automatically dropped freely onto the specimen at 15 min intervals, and Vicasoft personal computer software for data processing. Thirty percent slag replacement in CEM I (C2) was used. The setting times were determined at 20°C and 35°C, which was the maximum temperature allowed by the equipment close to the 38°C target.

Slag activity index (SAI)
The SAI was determined according to BS EN 15167-1 (BSI, 2006) (related to ASTM C 989 (ASTM, 2016)) and BS EN 197-1 (BSI, 2011). Compressive strengths using split halves of three mortar prisms (40 mm × 40 mm × 160 mm) were determined in line with BS EN 196-1 (BSI, 2005) at 7 and 28 d for the SAI computations. Compressive strength was measured using 3000 kN capacity ToniPact automatic compression test plant equipped with Servocon digital control.

Calorimetry
Heat of hydration was followed by isothermal conduction calorimetry using a Tam air calorimeter. Paste samples made up of 6 g of binder and 3 g of deionised water were mixed in 20 ml closed plastic ampoules on a vortex shaker for 2 min and transferred into the calorimeter sample channels. Corresponding quartz reference samples were placed in the reference channels. Data were obtained continuously for 28 d at 20°C and 38°C.
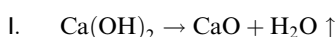
X-ray diffraction
The XRD analyses of hydrated pastes were performed using a Bruker D2 phaser diffractometer, scanning from 5° to 70° 2θ. A Cu Kα source was used, operating at 30 kV and 10 mA. The scan time was 2 s with a 0·034° increment and a sample

Advances in Cement Research
Volume 30 Issue 8

Performance of plain and slag-blended
cements and mortars exposed to
combined chloride–sulfate solution
Ukpata, Basheer and Black

rotation of 15/min, giving a total scan time of 4074 s. The crystalline phases in the binder samples were identified qualitatively by their characteristic diffraction patterns.

Simultaneous thermal analysis

The STA of hydrated pastes were performed using a Stanton Redcroft 780 series thermal analyser. Thermogravimetric analysis (TGA) and differential thermal analysis (DTA) data were obtained at temperatures of 20°C to 1000°C at a constant heating rate of 20°C/min, under nitrogen gas at flow rate of 50 ml/min. The initial weights of the binder powdered samples were kept between 15 and 17 mg. A corresponding empty platinum crucible was used as reference. Portlandite (CH) decomposed at about 400°C to 550°C according to Equation I

I. $\quad Ca(OH)_2 \rightarrow CaO + H_2O \uparrow$

The data obtained were used to calculate CH from the tangent method and bound water (W_b) contents. CH was normalised to the percent residual mass at 550°C. The %CH and W_b were computed using Equations 1–3

1. $\quad \%CH = CH_w \times \dfrac{M_{CH}}{M_{H_2O}}$

2. $\quad \%CH_{normalised} = \dfrac{\%CH}{W_{550}} \times 100$

3. $\quad W_b = \left(\dfrac{W_{50} - W_{550}}{W_{550}} \right) \times 100$

where %CH is the portlandite content (%); CH_w is the mass loss from portlandite (%); M_{CH} is the molar mass of portlandite (i.e. 74 g/mol); M_{H_2O} is the molar mass of water (i.e. 18 g/mol); $\%CH_{normalised}$ is the normalised portlandite content (%); W_b is the bound water (%); W_{50} is the residual mass at 50°C; and W_{550} is the residual mass at 550°C.

Flexural strength tests

Flexural strength tests were conducted in line with BS EN 196-1 (BSI, 2005). Flexural strengths were determined in triplicate using 25 kN Tinius Olsen equipment.

Sorptivity coefficients

Sorptivity coefficients were measured on cylindrical mortar samples measuring 28 mm dia. by 40 mm high. Samples were dried to constant mass at 40°C and, after cooling, the sides were coated with paraffin wax before being placed on a steel mesh suspended in deionised water at a laboratory temperature of 20 ± 1°C. The cut surfaces of the samples were kept in contact with water and submerged approximately 5 mm below the water surface. Masses were measured at specified times (i.e. 1, 4, 9, 16, 25, 36, 49 and 64 min) to determine the rate of

water absorption. Surface water on the sample was removed between successive measurements by placing the sample on a damp towel. Each measurement was completed within 30 s. The cumulative water absorbed i (g/mm²) is known to vary directly with the square root of time (min$^{-0.5}$), as shown in Equation 4, such that the slope of a plot of mass absorbed against the square root of time gives the sorptivity coefficient k ((g/mm²)/min$^{0.5}$) (BS EN 13057 (BSI, 2002); Guneyisi and Gesoglu, 2008; Sabir et al., 1998; Tasdemir, 2003) (related to ASTM C 1403 (ASTM, 2015)).

4. $\quad i = k\sqrt{t}$

where i is the cumulative water absorption (g/mm²); t is time (s); and k is the sorptivity coefficient ((g/mm²)/s$^{0.5}$)

Intrinsic gas permeability

Intrinsic gas permeability was measured on triplicate mortar cylinders (28 mm dia. × 40 mm high) prepared as described for the sorptivity test, using the Leeds permeameter, after Cabrera and Lynsdale (1988). The samples were fitted tight within the cells and connected to a nitrogen line at constant pressure of 1 bar. The cell is designed to allow unidirectional flow of gas through the samples and the flow rate was measured in flow meters by monitoring the time taken for water bubbles to travel under gas pressure through specified pressure heads. Three measurements were taken per sample to calculate the flow rate (cm³/s), from which the intrinsic gas permeability was calculated according to Equation 5.

5. $\quad K_i = \dfrac{2\mu Q L P_2}{A(P_1^2 - P_2^2)}$

where μ is the dynamic viscosity of gas at the test temperature (Ns/m²); Q is the volume flow rate of gas measured at pressure P_2 (m³/s); L is the length of specimen (m); A is the cross-sectional area of specimen; and P_1 and P_2 are the injection and exit pressures (Pa).

Total chloride profile

The total acid-soluble chloride concentrations in the mortar samples were determined according to Rilem TC 178-TMC (2002). The 1 g of powder sample obtained from ground mortar slices (Figure 2) was dissolved using 50 ml of 30% nitric acid. Then 5 ml or 10 ml of 0·05 M silver nitrate (AgNO₃) solution was added to precipitate chloride and filtered into a beaker to remove the solids. About 200 ml dilute nitric acid was used to wash the solids over the filter paper, and 20 drops of saturated ammonium iron III sulfate indicator solution were added to the solution. The solution was then titrated against ammonium thiocyanate (NH₄SCN) until there was a colour change. The concentration of chloride in the solution was then calculated using Equation 6. The calculated chloride contents (in wt %/g of dry mortar sample), were

Advances in Cement Research
Volume 30 Issue 8

Performance of plain and slag-blended
cements and mortars exposed to
combined chloride–sulfate solution
Ukpata, Basheer and Black

Table 5. Slag activity indices

Age: d	Slag 1 activity indices: %	Slag 2 activity indices: %	Requirement for good performance: %	Reference
7	80·4	77·2	≥45	BS EN 15167-1 (BSI, 2006)
28	95·1	85·1	≥70	BS EN 15167-1 (BSI, 2006)

Table 6. Setting times

Code	Binder	Setting times at 20°C: min		Setting times at 35°C: min	
		Initial	Final	Initial	Final
C1	CEM I 42.5R	360	480	245	330
C2	CEM I 52.5R	275	345	175	215
C2S1	70% CEM 52.5R + 30% Slag 1	300	460	205	290
C2S2	70% CEM 52.5R + 30% Slag 2	350	465	205	300

plotted against distances (mm) from the exposed surface to produce a chloride concentration profile.

6. $$\%\mathrm{Cl} = \frac{3 \cdot 5453 V_{\mathrm{Ag}} M_{\mathrm{Ag}}(V_2 - V_1)}{m V_2}$$

where V_{Ag} is the volume of silver nitrate added (cm^3); M_{Ag} is the molarity of the silver nitrate solution; V_1 and V_2 are the volumes of ammonium thiocyanate solution (cm^3) which were used in the sample and blank titrations, respectively; and m is the mass of powder sample (g).

The non-steady-state chloride diffusion coefficient was obtained by fitting the error function solution (Equation 7) of the diffusion equation (Equation 8) from Fick's second law of diffusion, which has been used by many researchers to describe the transport of chloride ions in cement and concrete systems (Wang *et al.*, 2016; Zhang and Zhang, 2014).

7. $$C(x, t) = C_{\mathrm{s}} - (C_{\mathrm{s}} - C_{\mathrm{i}})\mathrm{erf}\left(\frac{x}{2\sqrt{D_{\mathrm{a}}t}}\right)$$

8. $$\frac{\partial C}{\partial t} = -D\frac{\partial^2 C}{\partial x^2}$$

where $C(x, t)$ is the chloride ion concentration at a depth x from an exposed surface for time t; C_{s} is the surface chloride concentration; C_{i} is the initial chloride concentration of the mortar; erf is the error function; and D_{a} is the chloride diffusion coefficient (mm^2/year, or converted to m^2/s dividing by $3 \cdot 15576 \times 10^{13}$).

Results and discussion

Reactivity of the test slags
The reactivity of the test slags designated as slag 1 and 2 were evaluated using slag hydraulic indices (HIs) (Table 1), SAIs

(Table 5), setting times (Table 6) and hydration heat flows from calorimetry (Figures 3 and 4).

Slag activity indices (SAI)
Table 5 presents the SAI for slags 1 and 2, using the standard 50% slag replacement in CEM I (BS EN 15167-1 (BSI, 2006); BS EN 197-1 (BSI, 2011)). Both slags exceeded the requirements for good performance at both 7 and 28 d. Furthermore, the results confirm the greater reactivity of slag 1, both at early age and over longer times. These results generally agree with the HIs (Table 1), where both the extended and simple HI indicate that the more basic slag 1, with higher alumina content, is more reactive than slag 2, consistent with the SAI. Many authors have reported on the inability of the HI to reliably measure the potential performance of slags in composite cements. For instance, Otieno *et al.* (2014) argued that the HI was unreliable in measuring the performance of concrete resistance against chloride penetration, whereas Mantel (1994) concluded that HI could not predict the strength performance of slag cements effectively, but agreed that HI could be used to roughly predict the basicity of slags. Nevertheless, the HIs have demonstrated the influence of slag composition on the potential reactivities and performances of slags 1 and 2 in the blended cement systems and show good agreements with the activity indices and setting time results.

Setting times
The setting times (Table 6) for slag1 blend were shorter than slag 2, confirming slag 1's greater reactivity shown by the HI results. This is in line with the literature, where longer setting times have been attributed to lower alumina and/or higher magnesia contents of slags (Akın Altun and Yılmaz, 2002; Kourounis *et al.*, 2007). Increasing temperature from 20°C to 35°C caused a reduction in all setting times, but the reduction was particularly pronounced (over 30%) for the two slag blends. Comparing the setting times for the CEM I (C2) with those of slag blends shows that slags retard hydration. The
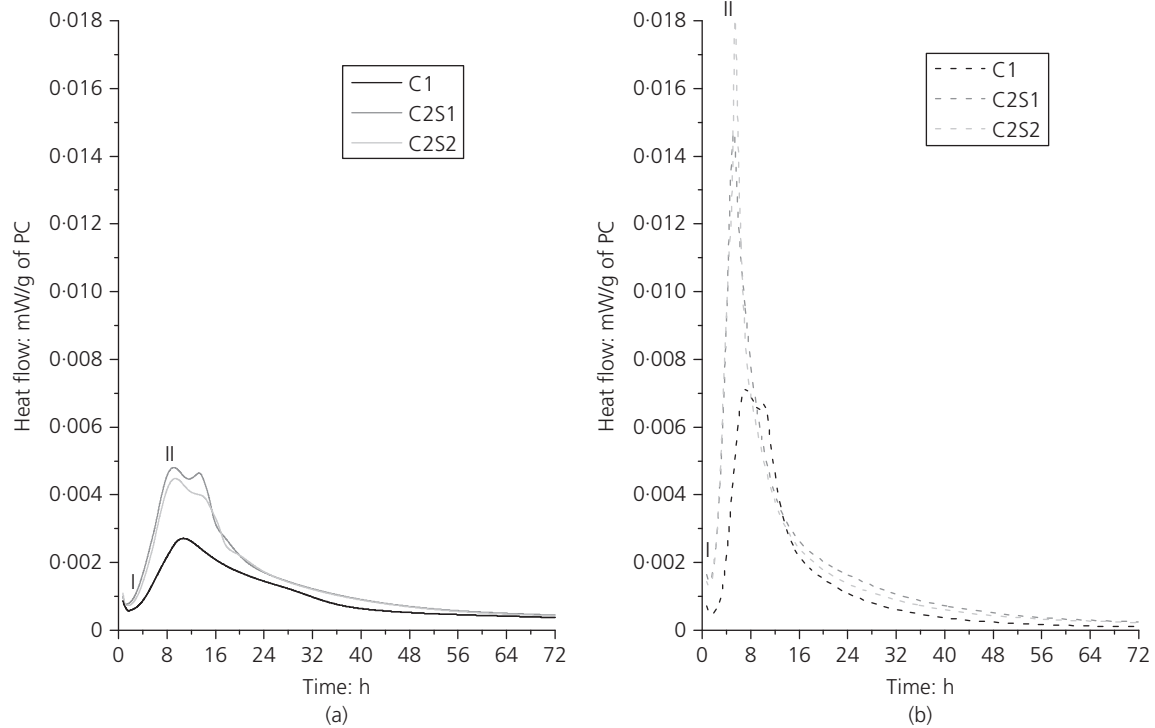
Advances in Cement Research
Volume 30 Issue 8

Performance of plain and slag-blended cements and mortars exposed to combined chloride–sulfate solution
Ukpata, Basheer and Black

Figure 3. Heat flow from test binders at: (a) 20°C; (b) 38°C

Figure 4. Total heat evolved by all test binders at 20°C and 38°C

Heat flow from isothermal conduction calorimetry

The heat flows due to hydration of the test binders at 20°C and 38°C are presented in Figures 3(a) and 3(b), respectively. Figures 3 and 4 show that increased temperature increased the reactivity of the slag blends, confirming earlier findings by other researchers (Barnett *et al.*, 2006; Escalante *et al.*, 2001; Ogirigbo and Black, 2016). The increased hydration is expected to reduce gel pores in the C–S–H, causing it to shrink, thereby increasing the surrounding capillary pores, which can lead to an increase in chloride diffusion, as shown later in Figure 12. For the slag blends hydrated at 20°C, the acceleration period was completed between 7 and 8 h (i.e. I to II), whereas for blends hydrated at 38°C the acceleration period (i.e. I to II) was complete between 4 and 6 h, respectively. The final setting times all fall within the acceleration periods and the rates of hydration of different binders generally correspond to setting time results. The cumulative heat flow for different binders (Figure 4) agrees with strength development (see Figure 9 later), increasing only slightly between 7 and 28 d.

Influence of combined chloride–sulfate solution on hydration characteristics

X-ray diffraction analysis
The XRD analyses were performed on hydrated paste samples exposed to the combined chloride (30 g/l)–sulfate (3 g/l) solution and compared with those exposed to water only.
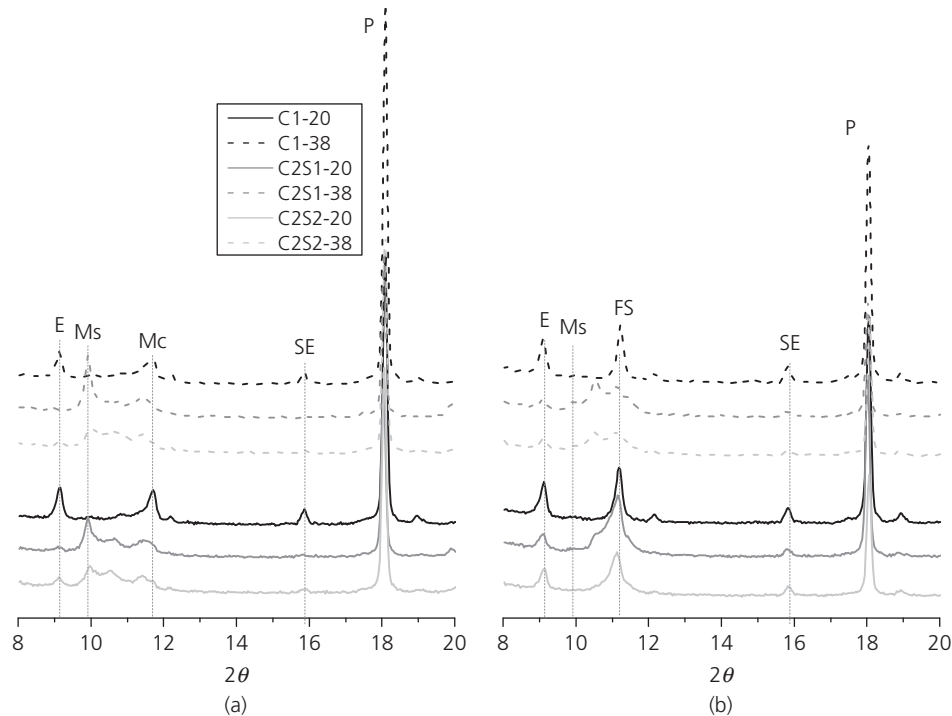
observed slow setting of C1 can be attributed to comparatively lower specific surface area of the cement (Table 3). The results at 20°C are generally higher than setting times data reported by Kourounis *et al.* (2007) for steel slag blended binders at 30% weight replacement, but agrees with the setting times determined at 35°C. The difference may be attributed to differences in temperature or other factors such as slag types, fineness and composition of cement used.

Advances in Cement Research
Volume 30 Issue 8

**Performance of plain and slag-blended
cements and mortars exposed to
combined chloride–sulfate solution**
Ukpata, Basheer and Black

Figure 5. XRD of different paste samples at 28 d: (a) immersed in water (X1); (b) immersed in combined solution of sodium chloride and sulfate (X2) after 7 d of pre-curing in water (note: E, ettringite or AFt; Ms, monosulfate; Mc, monocarboaluminate; Hc, hemicarboaluminate; SE, secondary ettringite; P, portlandite; FS, Friedel's salt)

Normally, CEM I hydration would produce the well-known hydration products as follow: hydration of C_2S and C_3S would produce CH and C–S–H, while C_3A and C_4AF would react with the sulfate present in the CEM I to form both AFt and AFm phases. With slag blends, various phases are formed including: C–S–H, C–A–S–H, AFm, AFt, hydrogarnet and a hydrotalcite-like phase (Chen and Brouwers, 2007; Hewlett, 2004; Kolani *et al.*, 2012).

However, Figures 5 and 6 show that exposure of relatively immature hydrated paste samples to a combined chloride and sulfate solution led to the formation of Friedel's salt (FS), monosulfate (Ms) and ettringite (E) after 28 and 90 d respectively. In Figure 5(b), an increase in curing temperature from 20 to 38°C led to diminishing peaks attributed to Friedel's salt and ettringite for the slag blends. The increased slag hydration at higher temperatures may have led to a more compact microstructure, hindering ingress of the salt solution. The reverse was observed for the CEM I, also consistent with the strength results (Figure 9).

Also, in the presence of the combined chloride–sulfate solution, monosulfate levels were depleted with an increased presence of ettringite in the slag blends. This was likely due to the reaction of aluminates with chlorides to form Friedel's salt. This tends to agree with Maes and De Belie (2014) that

chloride has a mitigating influence on sulfate attack. Santhanam *et al.* (2006) had also earlier reported that, in the presence of relatively high concentration of chloride, such as in seawater, there was a reduced tendency for sulfate expansion related to ettringite formation. It is also known that sulfate solubility decreases in chloride solutions.

Portlandite and bound water contents from thermal analysis

Portlandite content (CH)

Analysis of portlandite consumption has been found to be one of the promising techniques to determine the degree of slag hydration in blended systems (Durdziński *et al.*, 2017). Figures 7(a)–7(c) show portlandite contents from 7 to 90 d for all binders cured for 7 d at 20°C and 38°C then exposed to either the combined chloride–sulfate solution or water only. The presence of a salt solution contributed to a decrease in portlandite contents for some binders and an increase for others. Although the decrease in CH for the slag blends may be attributed to increased slag hydration (Bougara *et al.*, 2010; Kolani *et al.*, 2012; Ogirigbo and Black, 2016; Pane and Hansen, 2005), it indicates a decrease in hydration for the neat system (Escalante-García and Sharp, 1998; Ogirigbo, 2016). Also, the formation of Friedel's salt and AFt as confirmed by XRD analysis of the samples exposed to the salt solution
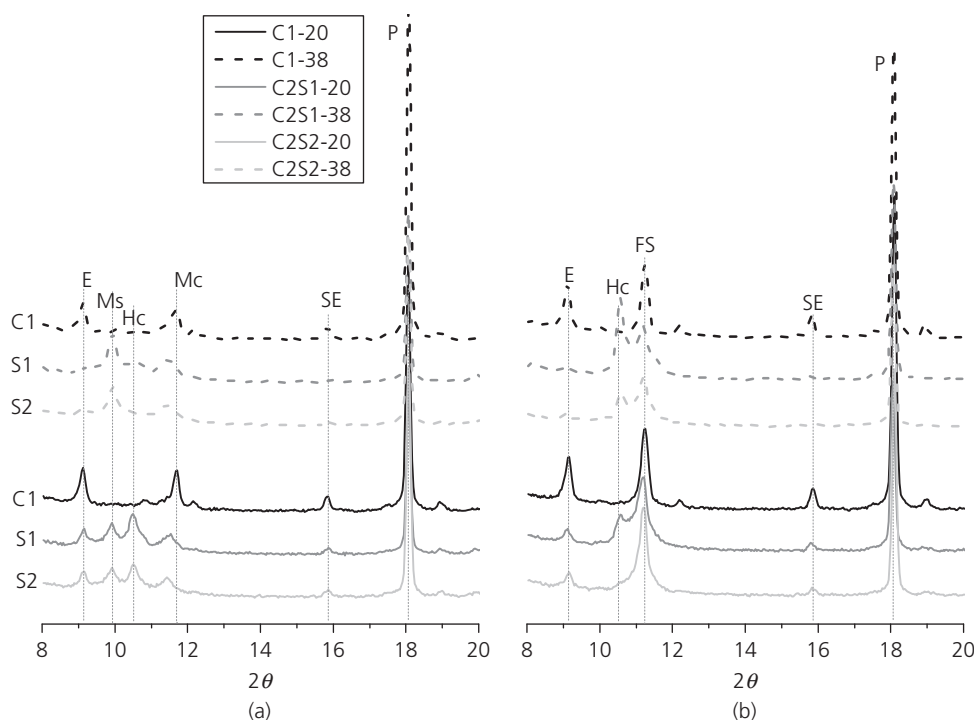
Advances in Cement Research
Volume 30 Issue 8

**Performance of plain and slag-blended
cements and mortars exposed to
combined chloride–sulfate solution**
Ukpata, Basheer and Black

Figure 6. XRD of different paste samples at 90 d: (a) immersed in water (X1); (b) immersed in combined solution of sodium chloride and sulfate (X2) after 7 d of pre-curing in water (note: E, ettringite or AFt; Ms, monosulfate; Mc, monocarboaluminate; Hc, hemicarboaluminate; SE, secondary ettringite; P, portlandite; FS, Friedel's salt)

(Figures 5(b) and 6(b)) would require a source of calcium from the CH, which can also explain the decrease in CH observed.

Bound water content (W_b)

The bound water contents at 7, 28 and 90 d, respectively, are presented in Figures 8(a), 8(b) and 8(c) for all binders at 20°C and 38°C exposure temperatures, showing samples exposed to the combined chloride (30 g/l)–sulfate (3 g/l) solution (X2) and those cured under water only (X1). W_b for samples cured under water followed a similar trend as the degree of hydration (Figure 4) and flexural strength development (Figure 9), increasing with time, in line with other studies (Ogirigbo and Black, 2016; Pane and Hansen, 2005), while W_b for samples exposed to X2 decreased at 28 d and 90 d. This demonstrates the futility of using bound water content to quantify the degree of hydration of binders which have been contaminated with other hydrates such as the Friedel's salt produced in the binder matrix as a result of chloride ingress. Thermal analysis of synthetic Friedel's salt by Grishchenko et al. (2013) has shown mass losses due to water removal at temperatures well beyond the 550°C limit generally used by most researchers for cement materials (Ogirigbo, 2016; Whittaker, 2014). Hence, no conclusion can be made concerning the effect of combined chloride–sulfate exposure on the degree of hydration of samples exposed to salt solution because part of the mass loss due to bound water in Friedel's salt was not considered.

Influence of combined chloride–sulfate exposure on mechanical properties

The influence of exposure to combined chloride–sulfate solution on the mechanical properties of mortar prisms can be seen in Figures 9(a)–9(c) showing flexural strength development from 7 through 28 to 90 d of hydration. The more basic, aluminum-rich slag 1 blend (Table 1) performed better than the slag 2 blend, consistent with the heat flow hydration characteristics from calorimetry data (Figure 4). Regarding the influence of temperature on mechanical properties, an increase in temperature from 20°C to 38°C led to consistent increase in flexural strengths of slag-blended mortars but caused strength loss in the CEM I. It is known that microstructure has an effect on strength. In CEM I, the hydration products – inner C–S–H – are densified at higher temperature, which leads to an increase in porosity and so a decrease in strength, despite the higher degree of hydration (Kjellsen et al., 1991; Lothenbach et al., 2007). In the slag blends, although this still occurred, it was more than compensated for by the greatly increased slag hydration.

Figures 9(b) and 9(c) show a comparison between flexural strengths at 28 and 90 d of mortars exposed to salt solution (X2) and those cured in water (X1). Exposure to the salt solution consistently caused an increase in flexural strengths for both CEM I and the slag blends. It is well known that chlorides
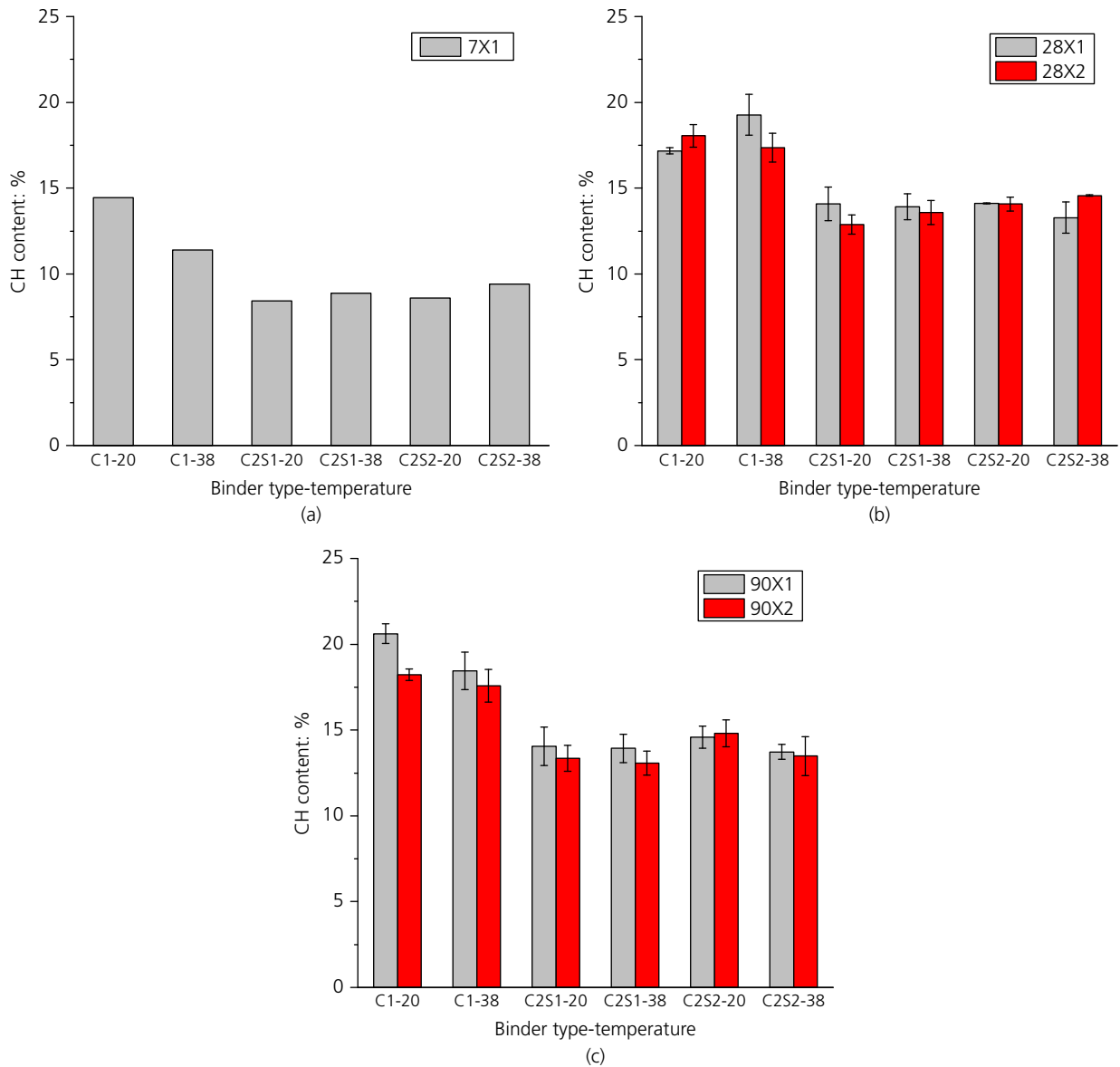
Advances in Cement Research
Volume 30 Issue 8

Performance of plain and slag-blended cements and mortars exposed to combined chloride–sulfate solution
Ukpata, Basheer and Black

Figure 7. Portlandite contents at: (a) 7 d; (b) 28 d; (c) 90 d

tend to activate the early-stage hydration, although the deliberate addition of chlorides during mixing is avoided because of the tendency for steel reinforcement bar corrosion (Galan and Glasser, 2015; Harrison, 1990; Ogirigbo and Ukpata, 2017). The increased strengths in the mortars exposed to the combined solution suggests a synergy between chloride and sulfate in refining the microstructure of the matrix, resulting in densification and increased strength in line with the findings of Frias *et al.* (2013). Chlorides and sulfates react with the aluminate phases in hydrated Portland cement to form Friedel's salt and ettringite, respectively. In slag blended cements, slag reactivity is activated by the presence of high concentration of chloride in the pore solution as sulfate is preferentially bound to the aluminates, causing the formation of hydrated aluminates of layered structure, which then transform to Friedel's salt through ionic exchange between hydroxide and chloride (Frias *et al.*, 2013). This causes a reduction in porosity, resulting in a more compact microstructure, which supports the increased flexural strengths observed (Caijun *et al.*, 2017; Divsholi *et al.*, 2014; Ehtesham Hussain and Rasheeduzzafar, 1994; Frias *et al.*, 2013; Goni *et al.*, 1994; Maes and De Belie, 2014).

Influence of combined chloride–sulfate solution on transport properties

Sorptivity coefficients
Figure 10 shows the measured sorptivity coefficients following hydration for 7 d and then exposure to either X1 or X2 up to
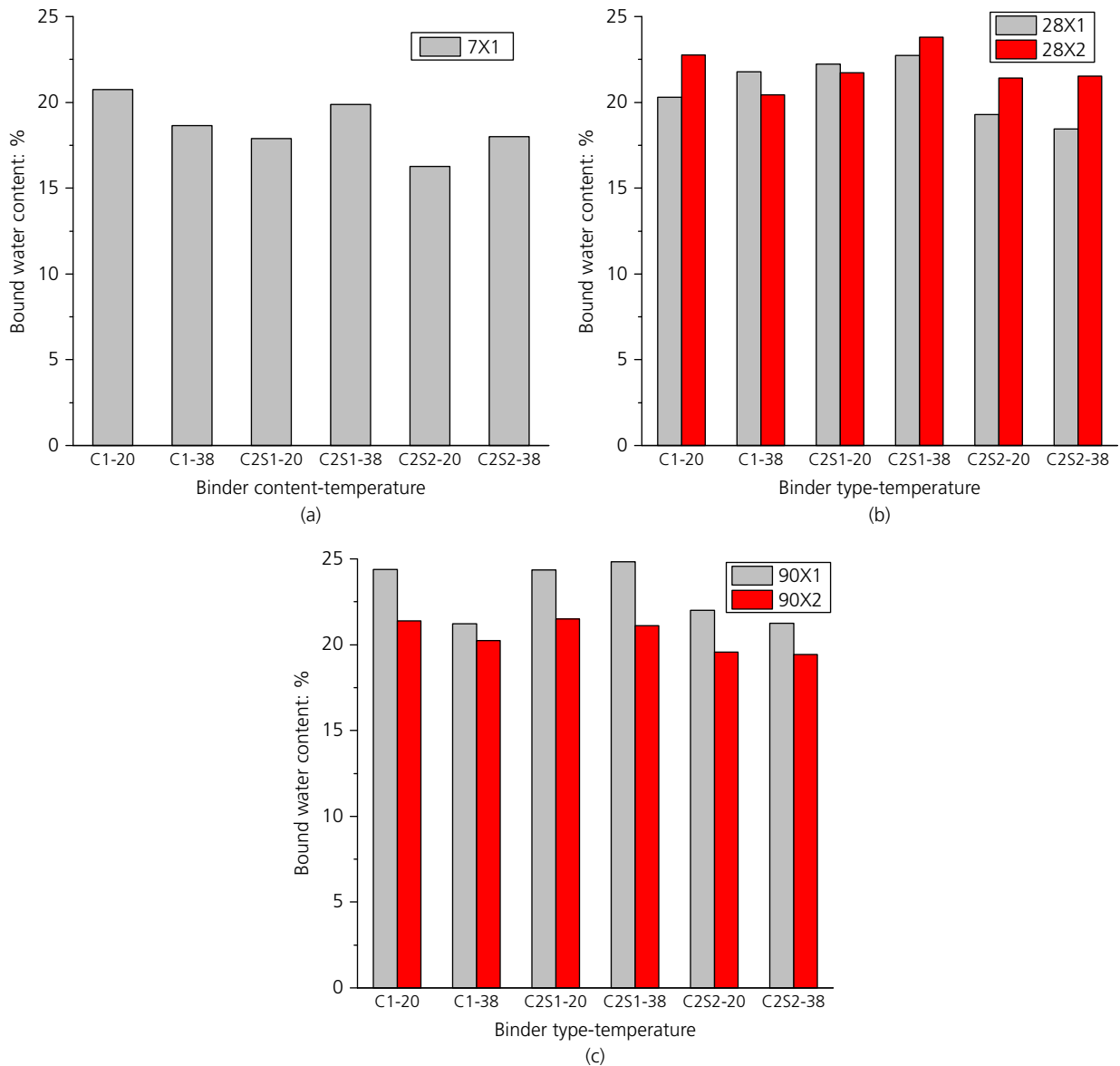
Advances in Cement Research
Volume 30 Issue 8

Performance of plain and slag-blended
cements and mortars exposed to
combined chloride–sulfate solution
Ukpata, Basheer and Black

Figure 8. Bound water contents at: (a) 7 d; (b) 28 d; (c) 90 d

a total age of 28 d. The figure illustrates the effects of curing conditions, binder composition and exposure conditions. Sorptivity reduces with an increase in curing temperature, as would be expected due to the increased degree of slag hydration (see calorimetry data). Somewhat surprisingly, incorporation of the less reactive slag 2 resulted in a binder with lower sorptivity at 20°C compared with slag 1. Generally, slag 2 with higher magnesium oxide content showed better sorptivity compared to slag 1, consistent with earlier findings where increase in magnesium oxide contents of slag have led to increased strength and reduced porosity (Haha *et al.*, 2011; Winnefeld *et al.*, 2015). This also mostly agrees with the gas permeability results shown in Figure 11.

All of the mixes showed a considerable decrease in sorptivity beyond 7 d following exposure to either water or salt solution. This reflects the incompletely developed microstructure after just 7 d, and the continued binder hydration upon immersion. Sorptivity showed a greater decrease following immersion in salt solution than following immersion in pure water. This reflects the increased degree of hydration induced by the chlorides and also the pore blocking effects of ettringite precipitation shown in XRD analysis (Figures 5 and 6).

Intrinsic gas permeability

Figure 11 shows the intrinsic gas permeability results. There was generally a good agreement between these data and the
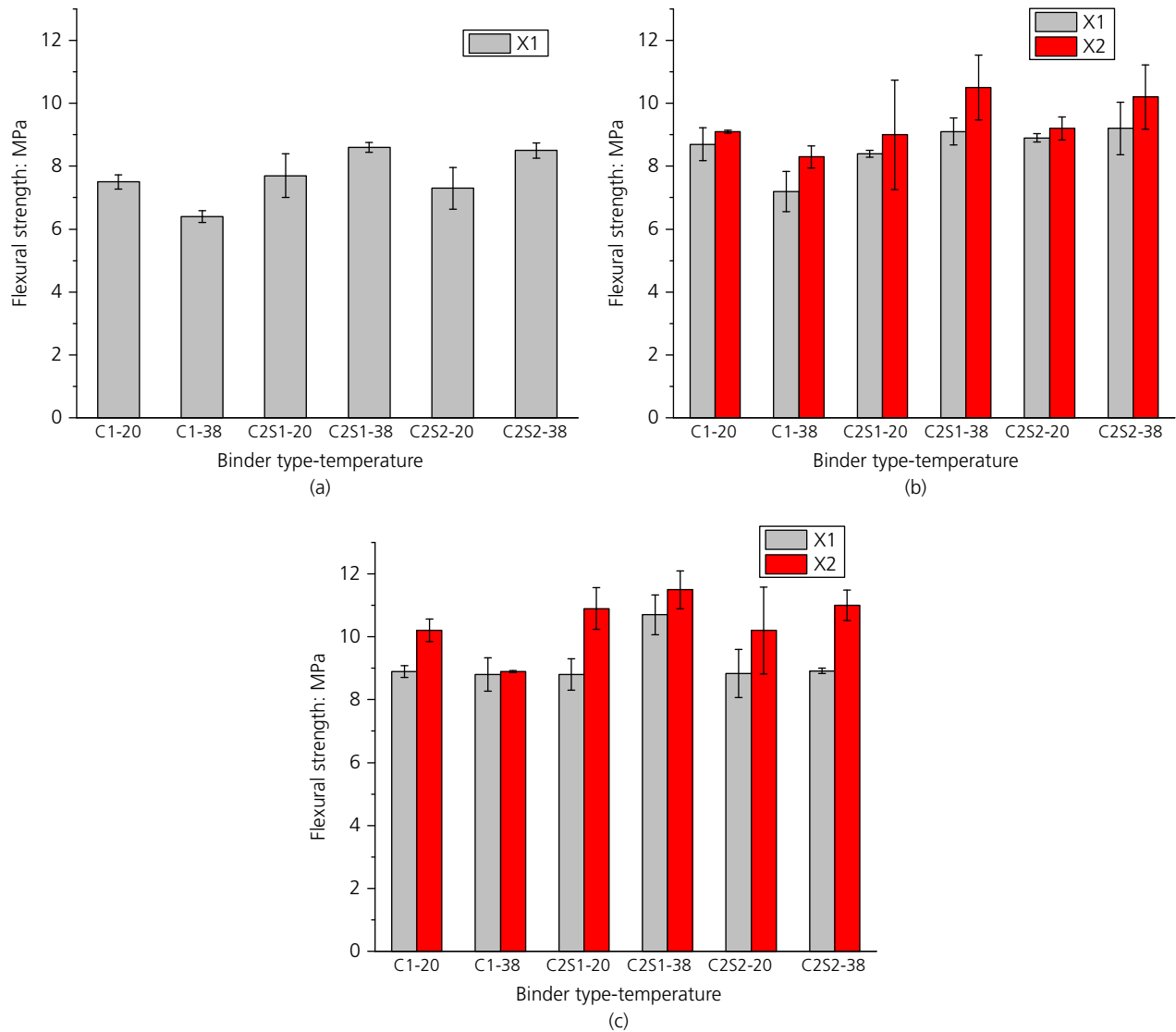
Advances in Cement Research
Volume 30 Issue 8

Performance of plain and slag-blended
cements and mortars exposed to
combined chloride–sulfate solution
Ukpata, Basheer and Black

Figure 9. Flexural strengths at: (a) 7 d; (b) 28 d; (c) 90 d for mortar samples cured in water (X1) and combined chloride–sulfate solution (X2)

sorptivity data presented earlier, apart from the slag blends cured at 20°C and then exposed to salt solutions. This may be due to the differences between the two mechanisms, as gas permeability is driven by external gas pressure with a tendency to give more pronounced results than sorptivity, which is only driven by the material's absorption capability. In all instances, the permeability decreased between 7 d and 28 d when immersed in water, reflecting the improved hydration. This was particularly true for slag hydration at 20°C, and less so at 38°C as the slag had already hydrated to a greater extent at the higher temperature prior to immersion. Meanwhile, higher curing temperatures of the CEM I mixes led to higher permeabilities, a result of the increased porosity witnessed under such curing conditions (Bahafid *et al.*, 2017; Escalante-García

and Sharp, 2001; Gallucci *et al.*, 2013; Kjellsen *et al.*, 1990; Lothenbach *et al.*, 2007).

Upon immersion in a salt solution, all CEM I mixes and the high-temperature slag mixes showed reduced permeabilities of up to 9% for CEM I, 75% for slag 1 blend and 66% for the slag 2. This trend is consistent with the flexural strength results shown earlier and indicates that the positive influence of the salt solution on mechanical and transport properties of the slag blends is more evident as slag hydration is activated at 38°C. The slag mixes cured at 20°C, however, showed increased permeabilities. This may be attributed to the damaging effect of high concentration of chloride on dissolution of CH and decalcification of C–S–H (Galan and Glasser, 2015; Henocq
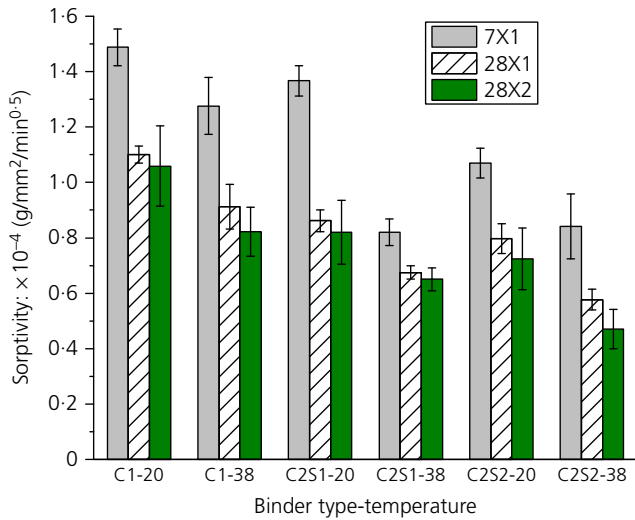
Advances in Cement Research
Volume 30 Issue 8

**Performance of plain and slag-blended
cements and mortars exposed to
combined chloride–sulfate solution**
Ukpata, Basheer and Black

Figure 10. Changes in sorptivity coefficients with age and the
influence of chloride–sulfate solution exposure between 7 and
28 d (note: X1 in the key represents curing under water; X2
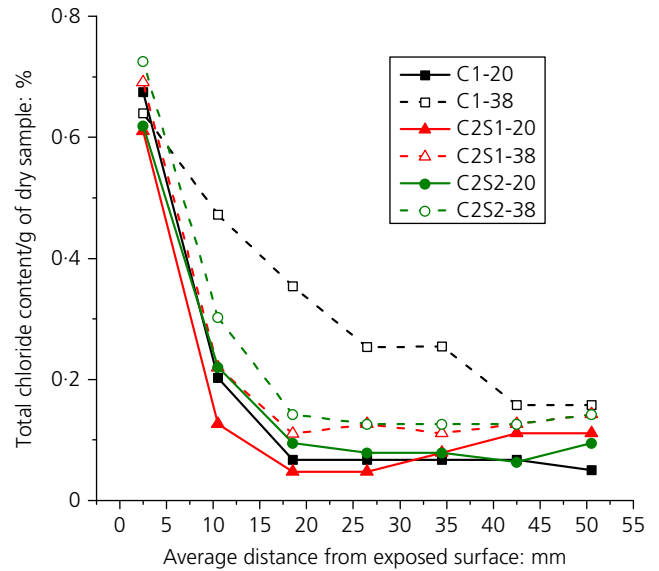represents submersion in chloride–sulfate salt solution)

Figure 12. Total chloride profile in mortar prisms exposed to
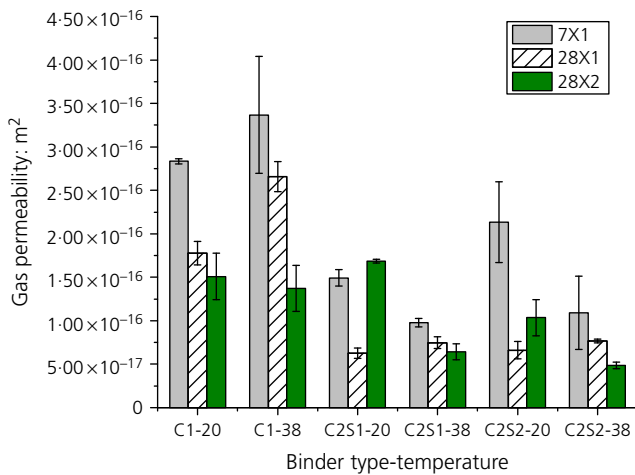combined chloride–sulfate solution at 20°C and 38°C

Figure 11. Changes in intrinsic gas permeability coefficients with
age and the influence of chloride–sulfate solution exposure
between 7 and 28 d

Table 7. Non-steady-state diffusion coefficients

		Diffusion coefficient:	
Binder	**Temperature: °C**	**m²/s × 10⁻¹²**	**Adj. R^2**
C1	20	3·869	0·97
C1	38	15·357	0·92
C2S1	20	1·807	−0·70
C2S1	38	1·820	0·79
C2S2	20	5·114	0·92
C2S2	38	4·512	0·98

et al., 2007) being possibly more pronounced while the degree
of slag hydration was still low at 20°C.

Total chloride profile analysis

Diffusion is a major mechanism for the transport of chloride
ions in submerged structures. Figure 12 shows the profiles of
total chloride contents with depths of unidirectional diffusion
after 90 d of submersion in combined chloride–sulfate sol-
ution, while Table 7 shows non-steady-state diffusion coeffi-
cients. At both temperatures of 20°C and 38°C, slag 1 was

more resistant to chloride penetration than slag 2, consistent
with slag reactivity discussed earlier. This also agrees with pre-
vious findings that higher alumina contents of slags would lead
to improved resistance through chloride binding (Dhir *et al.*,
1996; Ogirigbo and Black, 2015). Furthermore, the results
show that an increase in temperature generally led to increased
chloride diffusion in the samples, with the neat CEM I
mortars being the most affected. This is despite the increased
degree of hydration at higher temperatures (Figures 3 and 4)
and may be attributed to changes in microstructure with
coarser hydration products and densified inner C–S–H, follow-
ing increased hydration and the consequent increase in capil-
lary porosity, as discussed earlier for permeability.

Conclusions

■ This study has shown that in combined chloride
(30 g/l)–sulfate (3 g/l) solutions, slag-blended cement
mortars generally performed better with regards to
hydration, flexural strength and transport properties than
CEM I systems, especially at elevated temperatures (38°C).

Advances in Cement Research
Volume 30 Issue 8

Performance of plain and slag-blended
cements and mortars exposed to
combined chloride–sulfate solution
Ukpata, Basheer and Black

■ Exposure of CEM I systems and slag blends to a combined chloride–sulfate solution led to reductions in sorptivity and gas permeability, plus increases in flexural strengths, confirming the synergistic properties of chloride and sulfate in pore structure refinement reported by others. This effect was more pronounced at 38°C than at 20°C.

■ It appears that after longer exposure periods up to 90 d, chloride had a mitigating effect on sulfate attack, given the slightly reduced ettringite peaks observed from XRD analysis compared with increased Friedel's salt peaks over the same period. This agrees with the increasing flexural strength observed over the same period. Work to determine the depth of sulfate penetration is ongoing.

■ An elevated temperature of 38°C had a greater positive influence on the sorptivity, gas permeability and mechanical properties of slag blends than did slag composition. However, an increase in temperature appears to have a negative impact on these properties for CEM I systems, with or without exposure to salt water. This is due to changes in the microstructure of Portland cement causing increased porosity in spite of the accelerated hydration at 38°C.

■ The diffusion of chloride ions into mortars is influenced by temperature, with higher temperature leading to higher chloride diffusion. However, this did not correlate with sorptivity coefficients of the slag blends, which reduced with increase in temperature. This shows that temperature tends to have a greater influence on chloride transport in the slag cement mortars than the reduction in the pore system caused by it.

■ The more basic and more reactive slag 1 showed overall better resistance against chloride diffusion in spite of the slightly better sorptivity and gas permeability properties of slag 2, indicating a possible overriding influence of chloride binding by slag 1.

Acknowledgements

REFERENCES

Abdalkader AHM, Lynsdale CJ and Cripps JC (2015) The effect of chloride on cement mortar subjected to sulfate exposure at low temperature. *Construction and Building Materials* **78(1)**: 102–111.

Akın Altun İ and Yılmaz İ (2002) Study on steel furnace slags with high MgO as additive in Portland cement. *Cement and Concrete Research* **32(8)**: 1247–1249.

Al-Amoudi OSB, Maslehuddin M and Abdul-Al YAB (1995) Role of chloride ions on expansion and strength reduction in plain and blended cements in sulfate environments. *Construction and Building Materials* **9(1)**: 25–33.

ASTM (2010) C 1543: Standard test method for determining the penetration of chloride ion into concrete by ponding. ASTM International, West Conshohocken, PA, USA.

ASTM (2013) C 191: Standard test methods for time of setting of hydraulic cement by Vicat needle. ASTM International, West Conshohocken, PA, USA.

ASTM (2014) C 305: Standard practice for mechanical mixing of hydraulic cement pastes and mortars of plastic consistency. ASTM International, West Conshohocken, PA, USA.

ASTM (2015) C 1403: Standard test method for rate of water absorption of masonry mortars. ASTM International, West Conshohocken, PA, USA.

ASTM (2016) C 989: Standard specification for slag cement use in concrete and mortars. ASTM International, West Conshohocken, PA, USA.

Bahafid S, Ghabezloo S, Duc M, Faure P and Sulem J (2017) Effect of the hydration temperature on the microstructure of Class G cement: C–S–H composition and density. *Cement and Concrete Research* **95(1)**: 270–281.

Bai J, Wild S and Sabir BB (2003) Chloride ingress and strength loss in concrete with different PC–PFA–MK binder compositions exposed to synthetic seawater. *Cement and Concrete Research* **33(1)**: 353–362.

Bamforth PB, Price WF and Emerson M (1997) *An International Review of Chloride Ingress into Structural Concrete*. Transport Research Laboratory, Edinburgh, UK.

Barnett SJ, Soutsos MN, Millard SG and Bungey JH (2006) Strength development of mortars containing ground granulated blast-furnace slag: effect of curing temperature and determination of apparent activation energies. *Cement and Concrete Research* **36(13)**: 434–440.

Basheer L, Basheer PAM and Long AE (2005) Influence of coarse aggregate on the permeation, durability and the microstructure characteristics of ordinary Portland cement concrete. *Construction and Building Materials* **19(9)**: 682–690.

Bougara A, Lynsdale C and Milestone NB (2010) Reactivity and performance of blastfurnace slags of differing origin. *Cement and Concrete Composites* **32(4)**: 319–324.

BSI (2002) BS EN 13057: Products and systems for the protection and repair of concrete structures – test methods – determination of resistance of capillary absorption. BSI, London, UK.

BSI (2005) BS EN 196-1: Methods for testing cements. Part1: determination of strengths. BSI, London, UK.

BSI (2006) BS EN 15167-1: Ground granulated blast furnace slag for use in concrete, mortar and grout. Part 1: definitions, specifications and conformity criteria. BSI, London, UK.

BSI (2008) BS EN 196-3: Methods for testing cements. Part 3: determination of setting times and soundness. BSI, London, UK.

BSI (2011) BS EN 197-1: Cements part 1: Composition, specifications and conformity criteria for common cements. Part 1: composition, specifications and conformity criteria for common cements. BSI, London, UK.

BSI (2013) BS EN 206: Concrete – Specification, performance, production and conformity. BSI, London, UK.

BSI (2015a) BS 8500-1: Concrete – Complementary British Standard to BS EN 206. Method of specifying and guidance for the specifier. BSI, London, UK.

BSI (2015b) BS EN 12390-11: Testing hardened concrete. Part 11: determination of the chloride resistance of concrete, unidirectional diffusion. BSI, London, UK.

Cabrera JG and Lynsdale CJ (1988) A new gas permeameter for measuring the permeability of mortar and concrete. *Magazine of Concrete Research* **40(144)**: 177–182, http://dx.doi.org/10.1680/macr.1988.40.144.177.

Caijun S, Xiang H, Xiaogang W, Zemei W and Geert De S (2017) Effects of chloride ion binding on microstructure of cement pastes. *Journal of Materials in Civil Engineering* **29(1)**: 1–7.

Chen W and Brouwers HJH (2007) The hydration of slag, part 2: reaction models for blended cement. *Journal of Materials Science* **42(2)**: 444–464.

Advances in Cement Research
Volume 30 Issue 8

Performance of plain and slag-blended
cements and mortars exposed to
combined chloride–sulfate solution
Ukpata, Basheer and Black

De Weerdt K, Justnes H and Geiker MR (2014) Changes in the phase assemblage of concrete exposed to sea water. *Cement and Concrete Composites* **47(1)**: 53–63.

Dhir RK, El-Mohr MAK and Dyer TD (1996) Chloride binding in GGBS concrete. *Cement and Concrete Research* **26(12)**: 1767–1773.

Divsholi BS, Lim TYD and Teng S (2014) Durability properties and microstructure of ground granulated blastfurnace slag cement concrete. *International Journal of Concrete Structures and Materials* **8(8)**: 157–164.

Durdziński PT, Ben Haha M, Bernal SA *et al.* (2017) Outcomes of the RILEM round robin on degree of reaction of slag and fly ash in blended cements. *Materials and Structures* **50(2)**: 135.

Eglinton M (2004) Resistance of concrete to destructive agencies. In *Lea's Chemistry of Cement and Concrete, 4th edn* (Hewlett PC (ed.)). Elsevier Ltd, London, UK, pp. 299–342.

Ehtesham Hussain S and Rasheeduzzafar ASA (1994) Influence of sulfates on chloride binding in cements. *Cement and Concrete Research* **24(1)**: 8–24.

Escalante JI, Gomez LY, Johal KK *et al.* (2001) Reactivity of blast-furnace slag in Portland cement blends hydrated under different conditions. *Cement and Concrete Research* **31(1)**: 1403–1409.

Escalante-García JI and Sharp JH (1998) Effect of temperature on the hydration of the main clinker phases in Portland cements: part I, neat cements. *Cement and Concrete Research* **28(9)**: 1245–1257.

Escalante-García JI and Sharp JH (2001) The microstructure and mechanical properties of blended cements hydrated at various temperatures. *Cement and Concrete Research* **31(5)**: 695–702.

Frias M, Goñi S, García R and Villa RVDL (2013) Seawater effect on durability of ternary cements. Synergy of chloride and sulphate ions. *Composites. Part B, Engineering* **46(1)**: 173–178.

Galan I and Glasser FP (2015) Chloride in cement. *Advances in Cement Research* **27(2)**: 63–97, http://dx.doi.org/10.1680/adcr.13.00067.

Gallucci E, Zhang X and Scrivener KL (2013) Effect of temperature on the microstructure of calcium silicate hydrate (C–S–H). *Cement and Concrete Research* **53(1)**: 185–195.

Goni SM, Lorenzo P and Sagrera JL (1994) Durability of hydrated Portland cement with copper slag addition in NaCl + Na$_2$SO$_4$ medium. *Cement and Concrete Research* **24(8)**: 1403–1412.

Grishchenko RO, Emelina AL and Makarov PY (2013) Thermodynamic properties and thermal behavior of Friedel's salt. *Thermochimica Acta* **570(1)**: 74–79.

Guneyisi E and Gesoglu M (2008) A study on durability properties of high-performance concretes incorporating high replacement levels of slag. *Materials and Structures* **41(1)**: 479–493.

Haha MB, Lothenbach B, Le Saout G and Winnefeld F (2011) Influence of slag chemistry on the hydration of alkali-activated blast-furnace slag – part I: effect of MgO. *Cement and Concrete Research* **41(9)**: 955–963.

Haha MB, Lothenbach B, Le Saout G and Winnefeld F (2012) Influence of slag chemistry on the hydration of alkali-activated blast-furnace slag – part II: effect of Al$_2$O$_3$. *Cement and Concrete Research* **42(1)**: 74–83.

Harrison WH (1990) Effect of chloride in mix ingredients on sulphate resistance of concrete. *Magazine of Concrete Research* **42(152)**: 113–126, http://dx.doi.org/10.1680/macr.1990.42.152.113.

Henocq P, Samson E and Marchand J (2007) Effect of NaCl content in immersion solution on the decalcification of cement pastes. In *Proceedings of Rilem Workshop on Performance of Cement-based Materials in Aggressive Aqueous Environments: Characterization, Modelling, Test Methods and Engineering Aspects, Ghent, Belgium* (De Belie N) (ed.). Rilem, Paris, France, pp. 61–72.

Herrero T, Vegas IJ, Santamaría A, San-José JT and Skaf M (2016) Effect of high-alumina ladle furnace slag as cement substitution in masonry mortars. *Construction and Building Materials* **123**: 404–413.

Hewlett PC (ed.) (2004) *Lea's Chemistry of Cement and Concrete.* Elsevier Butterworth-Heinemann, Oxford, UK.

Holden WR, Page CL and Short NR (1983) The influence of chlorides and sulphates on durabilty. In *Corrosion of Reinforcement in Concrete* (Crane AP (ed.)). Ellis Horwood Limited, London, UK, pp. 143–150.

Kjellsen KO, Detwiler RJ and Gjørv OE (1990) Backscattered electron imaging of cement pastes hydrated at different temperatures. *Cement and Concrete Research* **20(2)**: 308–311.

Kjellsen KO, Detwiler RJ and Gjørv OE (1991) Development of microstructures in plain cement pastes hydrated at different temperatures. *Cement and Concrete Research* **21(1)**: 179–189.

Kolani B, Buffo-Lacarrière L, Sellier A *et al.* (2012) Hydration of slag-blended cements. *Cement and Concrete Composites* **34(9)**: 1009–1018.

Kourounis S, Tsivilis S, Tsakiridis PE, Papadimitriou GD and Tsibouki Z (2007) Properties and hydration of blended cements with steel making slag. *Cement and Concrete Research* **37(1)**: 815–822.

Kucharczyk S, Deja J and Zajac M (2016) Effect of slag reactivity influenced by alumina content on hydration of composite cements. *Journal of Advanced Concrete Technology* **14(1)**: 535–547.

Lothenbach B, Winnefeld F, Alder C, Wieland E and Lunk P (2007) Effect of temperature on the pore solution, microstructure and hydration products of Portland cement pastes. *Cement and Concrete Research* **37(1)**: 483–491.

Lothenbach B, Durdziński P and Weerdt KD (2016) Thermogravimetric analysis. In *A Practical Guide to Microstructural Ananlysis of Cementitious Materials* (Scrivener K, Snellings R and Lothenbach B (eds)). CRC Press, Taylor and Francis Group, London, UK, pp. 178–208.

Luo R, Cai Y, Wang C and Huang X (2003) Study of chloride binding and diffusion in GGBS concrete. *Cement and Concrete Research* **33(1)**: 1–7.

Maes M and De Belie N (2014) Resistance of concrete and mortar against combined attack of chloride and sodium sulphate. *Cement and Concrete Composites* **53(1)**: 59–72.

Mantel DG (1994) Investigation into the hydraulic activity of five granulated blast furnace slags with eight different Portland cements. *ACI Materials Journal* **91(5)**: 471–477.

Ogirigbo OR (2016) *Influence of Slag Composition and Temperature on the Hydration and Performance of Slag Blends in Chloride Environments.* PhD thesis, The University of Leeds, Leeds, UK.

Ogirigbo OR and Black L (2015) Chloride binding of GGBS concrete: influence of aluminium content, added sulphate and temperature. In *Proceedings of Ibausil International conference on Building Materials, Weimar, Germany* (Ludwig HM, Fischer HB, Boden C and Neugebaur M (eds)), pp. 1506–1513.

Ogirigbo OR and Black L (2016) Influence of slag composition and temperature on the hydration and microstructure of slag blended cements. *Construction and Building Materials* **126(1)**: 496–507.

Ogirigbo OR and Ukpata J (2017) Effect of chlorides and curing duration on the hydration and strength development of plain and slag blended cements. *Journal of Civil Engineering Research* **7(1)**: 9–16.

Otieno M, Beushausen H and Alexander M (2014) Effect of chemical composition of slag on chloride penetration resistance of concrete. *Cement and Concrete Research* **46(1)**: 56–64.

Pane I and Hansen W (2005) Investigation of blended cement hydration by isothermal calorimetry and thermal analysis. *Cement and Concrete Research* **35(6)**: 1155–1164.

Rilem TC 178-TMC (2002) Analysis of total chloride content in concrete. *Materials and Structures/Matériaux et Constructions* **35(1)**: 583–585.

Advances in Cement Research
Volume 30 Issue 8

Performance of plain and slag-blended
cements and mortars exposed to
combined chloride–sulfate solution
Ukpata, Basheer and Black

Sabir BB, Wild S and O'farrell M (1998) A water sorptivity test for
mortar and concrete. *Materials and Structures/Matériaux et
Constructions* **31(1)**: 568–574.

Santhanam M, Cohen M and Olek J (2006) Differentiating seawater and
groundwater sulfate attack in Portland cement mortars. *Cement
and Concrete Research* **36(1)**: 2132–2137.

Shen Q, Pan G and Zhan H (2017) Effect of interfacial transition zone
on the carbonation of cement-based materials. *Journal of
Materials in Civil Engineering* **29(7)**, pp. 1–9.

Sotiriadis K, Nikolopoulou E, Tsivilis S *et al.* (2013) The effect of
chlorides on the thaumasite form of sulfate attack of
limestone cement concrete containing mineral admixtures at low
temperature. *Construction and Building Materials* **43(1)**: 156–164.

Tasdemir C (2003) Combined effects of mineral admixtures and curing
conditions on the sorptivity coefficient of concrete. *Cement and
Concrete Research* **33(1)**: 1637–1642.

Wang Y, Li Q and Lin C (2016) Chloride diffusion analysis of concrete
members considering depth-dependent diffusion coefficients and
effect of reinforcement presence. *ASCE Journal of Materials in
Civil Engineering* **28(5)**: 1–9.

Whittaker MJ (2014) *The Impact of Slag Composition on the
Microstructure of Composite Slag Cements Exposed to Sulfate
Attack*. PhD thesis, University of Leeds, Leeds, UK.

Whittaker M and Black L (2015) Current knowledge of external
sulfate attack. *Advances in Cement Research* **27(9)**: 532–545,
http://dx.doi.org/10.1680/adcr.14.00089.

Whittaker M, Zajac M, Ben Haha M, Bullerjahn F and Black L (2014)
The role of the alumina content of slag, plus the presence
of additional sulfate on the hydration and microstructure of
Portland cement-slag blends. *Cement and Concrete Research*
66(1): 91–101.

Whittaker M, Zajac M, Ben Haha M and Black L (2016) The impact
of alumina availability on sulfate resistance of slag
composite cements. *Construction and Building Materials* **119(1)**:
356–369.

Winnefeld F, Haha MB, Saout GL *et al.* (2015) Influence of
slag composition on the hydration of alkali-activated
slags. *Journal of Sustainable Cement-Based Materials* **4(2)**:
85–100.

Zhang Y and Zhang M (2014) Transport properties in unsaturated
cement-based materials – a review. *Construction and Building
Materials* **72(1)**: 367–379.

Zuquan J, Wei S, Yunsheng Z, Jinyang J and Jianzhong L (2007)
Interaction between sulfate and chloride solution attack of
concretes with and without fly ash. *Cement and Concrete Research*
37(1): 1223–1232.

How can you contribute?

To discuss this paper, please submit up to 500 words to the editor at journals@ice.org.uk. Your contribution will be forwarded to the author(s) for a reply and, if considered appropriate by the editorial board, it will be published as a discussion in a future issue of the journal.